The Evaporation Kinetics of Pure Water Droplets at Varying Drying Rates and the Use of Evaporation Rates to Infer the Gas Phase Relative Humidity

Yong-yang Su†*, Rachael E. H. Miles‡, Zhi-ming Li†, Jonathan P. Reid‡, Jiang Xu†

† Northwest Institute of Nuclear Technology, P.O. Box 69-14, Xi'an, 710024, Shaanxi, PR China

‡ School of Chemistry, University of Bristol, Bristol, BS8 1TS, UK

Abstract

Numerous analytical models have been applied to describe the evaporation/condensation kinetics of volatile components from aerosol particles for use in many applications. However, the applicability of these models for treating cases that lead to substantial and rapid changes in particle temperature due to, for example, evaporative cooling remain to be compared with measurements. We consider three typical treatments, comparing predictions of the evaporation rates of pure water droplets over a wide range in gas phase relative humidity (RH) and exploring the sensitivity of the predictions to uncertainties in the thermophysical gas and condensed-phase parameters. We also compare predictions from the three treatments to measurements of the evaporation rates of pure water droplets with varying RH using an electrodynamic balance (EDB), concluding that only two of the model treatments are sufficiently able to account for the level of evaporative cooling (typically as high as 12 K). Finally, we show that the RH can be inferred accurately from the evaporation rate of pure water droplets over the full range in accessible RH and comparison with the model predictions (within absolute uncertainties of 2.5 % RH over the range 20% to 95 % RH), considering the level of agreement with independent measurements

made through determining the equilibrated size of aqueous sodium chloride and sodium nitrate droplets.

Keywords: Evaporation kinetics; model; Water droplet; Varying drying rates; Relative Humidity (RH); Single-particle technique.

1 Introduction

Predicting the kinetics of condensation and evaporation of volatile components from aerosol droplets is important in a broad range of applications, from predicting rates of droplet drying and loss of solvent in a spray drier and in consumer products[1], to the condensation kinetics of water in activating aerosol particles forming cloud droplets[2–4], and in the delivery of drugs from pressurized metered dose inhalers and nebulisers[5–7]. In many of these contexts, there is little direct experimental verification of microphysical models for predicting condensation and evaporation rates. Notable exceptions include the many measurements that have been made of water condensation kinetics on water droplets and, conversely, the evaporation kinetics[8,9]. Measurements can be divided into two types, those that probe the evolution of an entire size distribution[10,11] and those that examine the mass transfer kinetics at the level of an individual particle[12,13]. While the former have been used to examine condensation kinetics even in a supersaturated gas phase environment, aerosol particle samples have inherent polydispersity and the evolving size may only be measured at a final point in time or with coarse time-resolution. In single droplet studies, it has been suggested that measurements can be compromised by sample/surface impurities[9]. In both cases, an accurate measurement of the gas phase composition is essential to interpret and model the condensation/evaporation kinetics. For example, small uncertainties in the gas phase relative humidity (RH), also referred to as the degree of saturation (RH/100), can have a significant

impact on simulated mass transfer rates, and can compromise, for example, estimations of quantities such as the mass accommodation coefficient[14].

At the microphysical level, the framework for predicting droplet evaporation/condensation kinetics must include the competition between surface exchange (e.g. mass and thermal accommodation coefficients) and mass transport in the gas phase[15,16]. In the limit of large particle size, the Knudsen number is <<1 at atmospheric pressure and the condensation/evaporation process is limited by transport in the gas phase. In this limit, and assuming a steady temperature, the diffusional mass flux, driven by the difference between the partial pressure of the volatile component at infinite distance and the vapour pressure of the component above the droplet surface, can be estimated from an equation attributed to Maxwell[15]. Uncertainties in gas phase diffusion coefficients, vapour pressures, gas velocities and particle size must be fully accounted for in any prediction[14]. For droplets smaller than ~200 nm at atmospheric pressure, the Knudsen number is >>1 and the molecular nature of the interfacial exchange (as defined by the Hertz-Knudsen equation) must be accounted for recognizing, for example, that not every collision of a gas-phase condensing molecule with the surface may lead to accommodation and that the mass accommodation coefficient may be <1[8,17].

In both the limits of high and low Knudsen number, the interplay of heat and mass transport must be considered[15]. For example, a high mass flux from an evaporating droplet may lead to evaporative cooling, suppressing the droplet temperature, thereby suppressing the evaporation rate and mass flux. This coupling between heat and mass transfer must be incorporated in the framework used to simulate mass transfer rates. As a result, uncertainties in the thermophysical properties of the gas phase must be

fully quantified and accounted for when interpreting experimental data[14]. Although numerous comparisons between experiments and models have been performed with limited temperature differences between an aqueous droplet and surrounding vapour (e.g. see[14,18–23] for measurements where the temperature difference is <3 K), more extensive comparisons in the limit of rapid droplet evaporation/condensation and more significant differences in temperature would be valuable. Indeed, despite the anticipated simplicity of measuring and predicting the evaporation kinetics of pure water droplets, a refined microphysical description of the evaporation process that provides accurate predictions over a wide range in conditions is still lacking[8,24–26]. Thus, the purpose of this publication is to assess the performance of models for the evaporation of pure water droplets, initially ~25 μm in radius, into dry nitrogen at room temperature. Under these conditions, the droplet lifetime may be only ~2 s and temperature suppressions much greater than 3 K can be expected.

As a single particle levitation technique, the Electrodynamic Balance (EDB) is capable of trapping charged droplets in an electrical field and measuring the time-dependence of parameters such as droplet size and composition[27,28]. By fitting the time-dependent size using an appropriate model, the physical properties of materials, e.g. vapour pressure, evaporation coefficient, diffusion coefficient and hygroscopicity, can be measured[28]. Indeed, we have used the EDB technique previously to explore the evaporation kinetics of pure water droplets, estimating the vapour pressure of pure water down to 248 K[20] and determining limits for the evaporation coefficient[14,20], assumed equal to the mass accommodation coefficient by microscopic reversibility. We have also used the EDB technique to infer the hygroscopic growth curve of solutes up to very high water activity (>0.995) from the evaporation kinetics measurements[21–23,29]. In all of these cases, we have use a semi-analytical treatment for droplet

evaporation provided by Kulmala et al.[30] (referred to as the Kulmala model below), a valid approach provided the temperature suppression during evaporation does not exceed 3 K. This limits the accessible range of drying rates that can be modelled and, as a consequence, the lowest RH and highest temperature of the gas phase that drying can be studied at.

In this study we will compare the performance of the Kulmala model with two further models that should provide a more accurate treatment of evaporation rates even at much larger temperature suppressions. Ahn and Liu[31] developed a model (referred to as the Liu model) considering the coupled mass and heat transfer. This model was further modified by Su et al.[32] by taking into account the enhancement of the interfacial mass flux due to the relative movement between the levitated droplet and the flowing gas. Further, Kulmala and Vesala[33] and Heidenreich[34] developed a model (referred to as the K-V-H model) to describe condensation of a single-component droplet in the continuum regime, comprehensively taking into account the effects of Stefan flow, thermal diffusion and the Dufour effect.

As an additional benefit to providing a more comprehensive and accurate model framework for treating the evaporation of water droplets over a broader range of drying rates and environmental conditions, we anticipate that this refined model will improve the accuracy with which we are able to make hygroscopicity measurements. Our ability to measure the hygroscopic growth of a solute containing aerosol droplet (referred to as the sample droplet) to very high water activity and over very short time frame is dependent on an extremely accurate characterization of the gas phase RH[21,22]. This is achieved by using a probe droplet of known hygroscopic response, and thus evaporation kinetics profile, to infer the RH. This is a much more accurate method for determining the RH than conventional sensors such

as capacitance probes[29]. Indeed, unlike other probes, the RH measured in this way becomes increasingly accurate as the RH is increased. At the very highest RHs accessed in our measurements we use the evaporation kinetics of a water probe droplet to infer the difference between the gas phase saturation and the droplet vapour pressure, and thus the RH. However when using the Kulmala model, this becomes increasingly inaccurate as the RH decreases, the evaporation rate of the water droplet increases and, thus, the temperature suppression of the droplet increases beyond 3 K[21]. We will show that the refined model we present here allows us to retrieve the gas phase saturation over a much wider RH range as it accounts for this temperature suppression directly.

In Section 2, we derive a corrected form of the K-V-H model by considering the transitional correction for connecting the regimes of free-molecule to continuum range transport along with the impact of a flowing gas phase over a stationary droplet. We also examine of the sensitivity of K-V-H model prediction to the thermophysical properties (the diffusion coefficient, D_v, and thermal conductivity, K) and kinetic parameters (mass accommodation coefficient, α_M, and thermal diffusion factor, α_D), yielding a plausible range for α_D. In Section 3, we evaluate the performances of the Kulmala model, the Liu model and the K-V-H model by comparing their predictions of the evaporation profiles of water droplets under different RH conditions. In Section 4, we report new measurements of the evaporation kinetics of water droplets at varying RH using the EDB, and use the three models to obtain the corresponding RH, assessing the performance of the three models. Finally, we present comparative measurements of the evaporation profiles of aqueous NaCl or $NaNO_3$ droplets and pure water droplets under dry conditions, comparing the consistency of the inferred environmental conditions from the evaporation profiles of these two types of probe droplet.

2 Evaporation Models

2.1 Expressions of Mass Flux and Heat Flux

The mass flux, I, at the droplet surface during evaporation is defined by

$$I = -\frac{dm}{dt} = -4\pi\rho r^2 \frac{dr}{dt} \qquad (1)$$

where m, ρ and r are the mass, density and radius of the droplet, respectively. We now describe three models for estimating the size and time-dependence of the mass flux that we evaluate further in this paper.

2.1.1 The Kulmala Model

In the Kulmala model, the mass flux from a droplet evaporating in to a flowing gas is expressed as[14,30]

$$I = -4\pi r(S_\infty - a_w)\frac{Sh}{2}\left[\frac{RT_\infty}{\beta_M M_v D_v p_{eq}(T_\infty)A} + \frac{a_w L^2 M_v}{\beta_T R K T_\infty^2}\right]^{-1} \qquad (2)$$

where S_∞ is the saturation ratio in the gas phase far from the droplet, a_w is the water activity of the droplet (equal to unity for pure water droplets), R is the gas constant and T_∞ is the gas phase temperature far from the droplet. M_v is the molar mass of the evaporating species (in this case water), D_v is the diffusion coefficient of water in the carrier gas (composed of water vapour and nitrogen) and p_{eq} is the saturation vapour pressure of water. A is the Stefan flow correction factor (very close to unity under the conditions investigated), L is the latent heat of water, K is the thermal conductivity of the carrier gas, β_M and β_T are the Fuchs-Sutugin transitional correction factors for mass and heat transfer, respectively. The Sherwood number, Sh, is expressed as[25]

$$Sh = 2 + 0.6\left(\frac{2V_g r}{\nu_{N_2}}\right)^{1/2}\left(\frac{\nu_{N_2}}{D_v}\right)^{1/3} \qquad (3)$$

where V_g is the gas flow velocity and ν_{N2} is the kinematic viscosity of the gas.

The surface temperature of the droplet, T_d, can be estimated by

$$T_d = T_\infty - \frac{IL}{4\pi r K_\infty \beta_T} \qquad (4)$$

where K_∞ is the thermal conductivity of the gas far from the droplet. Equation (3) is valid only when the difference between the droplet surface temperature and the gas phase temperature is less than 3 K. Although the dependence of the droplet vapour pressure on temperature can be calculated accurately from the Clausius-Clapeyron equation, the Kulmala model approximates the exponential term by the first term in a Taylor series expansion. When the difference between the droplet surface temperature and the gas phase temperature exceeds 3 K, this approximation introduces significant error to the estimated value of the mass flux[21].

2.1.2 The Liu Model

In the Liu model, the droplet radius and the droplet temperature at the surface as a function of time are expressed as[32]

$$r\frac{\mathrm{d}r}{\mathrm{d}t} = \frac{Sh}{2}\frac{D_v M_v}{\rho R}\left(\frac{p_\infty}{T_\infty} - \frac{p_d}{T_d}\right)\beta_M \qquad (5)$$

$$T_d - T_\infty = \frac{Sh}{2}\frac{LD_v M_v}{KR}\left(\frac{p_\infty}{T_\infty} - \frac{p_d}{T_d}\right)\frac{\beta_M}{\beta_T} \qquad (6)$$

Where p_∞ and p_d are the partial pressures of the vapour far from and at the droplet surface, respectively.

2.1.3 The K-V-H Model

The mass flux of evaporation for a stagnant droplet in the continuum regime can be expressed as[33]

$$I_c = -\frac{4\pi r D_v(T_\infty) M_v p_t}{RT_\infty}\left[C_1 \ln\frac{1-p_d/p_t}{1-p_\infty/p_t} + C_2\frac{\alpha_D}{2}\left(\frac{p_\infty}{p_t} + \frac{p_d}{p_t}\right)\right] = I_{c1} + I_{c2} \qquad (7)$$

where I_{c1} is the mass flux component generated by the concentration gradient in the evaporating species between the droplet and the far field, and I_{c2} is the mass flux component generated by the temperature

gradient between the droplet and the far field. The latter is also called the thermal diffusion effect. α_D is the thermal diffusion factor and p_t is the total pressure. The coefficients C_1 and C_2 in Equation (7) are defined by

$$C_1 = \frac{(2-\mu)(1-f)}{1-f^{2-\mu}} \qquad (8)$$

$$C_2 = \frac{(3-\mu)(1-f)^2}{1-f^{3-\mu}} \qquad (9)$$

where f is defined as T_d/T_∞. μ is the exponential factor in the expression of D_v as a function of temperature. The μ value is usually between 1.5 and 2 depending on temperature and composition[35]. For water diffusing in nitrogen under atmospheric pressure and room temperature, the proposed value of μ is 1.81[36].

Heidenreich (1994)[34] derived an expression of heat transfer in the continuum regime in spherical coordinates:

$$Q_c = H_l I_c = -4\pi z^2 K \frac{dT}{dz} + H_v I_c + \alpha_D BRTI_c \qquad (10)$$

The $H_l I_c$ term represents the heat flux at the droplet surface at equilibrium. The $-4\pi z^2 K \frac{dT}{dz}$, $H_v I_c$ and $\alpha_D BRTI_c$ terms are components generated from thermal conduction, vapour mass diffusion and Dufour effect, respectively. H_l and H_v are the specific enthalpies of liquid water and water vapour, respectively. B is the correction factor accounting for the Dufour effect and is defined by

$$B = \frac{x_v x_g}{x_v M_v + x_g M_g}\left(\frac{x_g M_g}{x_v M_v} + 1\right) = \frac{x_g}{M_v} \qquad (11)$$

where x_v and x_g are the mole fractions of water vapour and nitrogen gas, respectively, and can be defined by $x_v=p_v/p_t$ and $x_g=p_g/p_t$ when both species behave as an ideal gas. x_v and x_g equal 0.023 and 0.977, respectively, at RH=100%, and 0 and 1 at RH=0%. Hence, B is 0.054278 at RH=100% and 0.055556 at RH=0%. Under the conditions investigated in this work (0<RH<100% and atmospheric pressure), B

can be treated as a constant.

Equation (10) is rearranged as

$$[H_v(T) - H_l(T_d) + \alpha_D BRT] \cdot I_c = 4\pi z^2 K \frac{dT}{dz} \qquad (12)$$

After variance separation, Equation (12) is changed to

$$\int_r^{\infty} \frac{I_c}{4\pi z^2} dz = \int_{T_d}^{T_\infty} \frac{K(T)}{H_v(T) - H_l(T_d) + \alpha_D BRT} dT \qquad (13)$$

Within a limited temperature range, the thermal conductivity, K, and the enthalpy of vaporization, H_v, vary linearly with temperature[34], so they can be expressed as

$$K = K_0 + K_1 \cdot T \qquad (14)$$

$$H_v(T) = H_v(T_d) + c_p \cdot (T - T_d) \qquad (15)$$

where c_p is the specific heat capacity of water vapour at constant pressure. The parameterization of c_p as a function of temperature is given in the CRC Handbook[37]. We can define

$$A_0 = H_v(T_d) - H_l(T_d) - c_p T_d = L(T_d) - c_p T_d \qquad (16)$$

$$A_1 = c_p + \alpha_D BR \qquad (17)$$

By using Equation (14) - (17), Equation (13) can be changed to

$$\int_r^{\infty} \frac{I_c}{4\pi z^2} dz = \int_{T_d}^{T_\infty} \frac{K_0 + K_1 T}{A_0 + A_1 T} dT \qquad (18)$$

After integration

$$\frac{I_c}{4\pi r} = \frac{1}{A_1}\left[\left(K_0 - \frac{K_1 A_0}{A_1}\right) \ln \frac{A_0 + A_1 T_\infty}{A_0 + A_1 T_d} + K_1 (T_\infty - T_d)\right] \qquad (19)$$

Therefore,

$$T_d = T_\infty - \frac{I_c A_1}{4\pi r K_1} + \left(\frac{A_0}{A_1} - \frac{K_0}{K_1}\right) \ln \frac{A_0 + A_1 T_d}{A_0 + A_1 T_\infty} \qquad (20)$$

In the transitional regime, the mass flux (I_T) and heat flux (Q_T) must be corrected by transition correction factors (refer to section 2.3.1) and can be written as[16]

$$I_{\mathrm{T}} = \beta_M I_c \qquad (21)$$

$$Q_T = \beta_T Q_c \qquad (22)$$

Taking into account the mass flux enhancement due to the relative movement between the droplet and a flowing gas[25], Equation (21) can be corrected to

$$I = \frac{Sh}{2}\beta_M I_c \qquad (23)$$

According to the definitions of Equation (22) and (23), I_c in the left-hand-side in Equation (12) is replaced by $\left(\frac{Sh}{2}\beta_M I_c\right)$, while the right-hand-side is corrected by a factor of β_T. After separating variances,

$$\int_r^{\infty} \frac{Sh}{2}\frac{\beta_M}{\beta_T}\frac{I_c}{4\pi z^2}dz = \int_{T_d}^{T_\infty} \frac{K(T)}{H_v(T)-H_l(T_a)+\alpha_D BRT}dT \qquad (24)$$

Comparing with Equation (13), a correction factor of $\left(\frac{Sh}{2}\frac{\beta_M}{\beta_T}\right)$ is introduced in the left-hand-side of Equation (24). Because this factor is independent of *r*, Equation (24) is integrated as

$$\frac{Sh}{2}\frac{\beta_M}{\beta_T}\frac{I_c}{4\pi r} = \frac{1}{A_1}\left[\left(K_0 - \frac{K_1 A_0}{A_1}\right)\ln\frac{A_0+A_1T_\infty}{A_0+A_1T_d} + K_1(T_\infty - T_d)\right] \qquad (25)$$

Typically, the correction factor can take values of up to 1.08 for the water droplet evaporation measurements presented here. For a gas velocity of 3 cm s^{-1}, a droplet size of 25 μm radius and a gas phase saturation ratio of 0.2, the surface temperature of the droplet can be estimated to be 281.1 K and the correction factor is 1.084. This factor has been used widely in previous publications[14,15,20,21,25,32].

Finally,

$$T_d = T_\infty - \frac{I_c A_1}{4\pi r K_1}\frac{Sh}{2}\frac{\beta_M}{\beta_T} + \left(\frac{A_0}{A_1} - \frac{K_0}{K_1}\right)\ln\frac{A_0+A_1T_d}{A_0+A_1T_\infty} \qquad (26)$$

The expressions for the estimation of T_d in the Kulmala model and the Liu model (refers to Equation (4) and (6)) are actually identical, both assuming *K* and H_v are constants. Comparatively, *K* and H_v are assumed to vary linearly with temperature in the K-V-H model.

2.2 The Thermophysical Properties

Expressions for the thermophysical properties of water and nitrogen used in the comparison of the three models are listed in Table 1. The origin of each expression, and any uncertainty associated with it, is discussed below.

2.2.1 Vapour Pressure of Water, p_{eq}

The parameterization for the vapour pressure of water, p_{eq}, listed in Table 1, is applicable between 123 K and 332 K[38]. The relative error in the calculated value of p_{eq} stated by the authors is less than 0.05% and, thus, the influence of this error on the accuracy of the three model predictions is not considered in this work.

2.2.2 Diffusion Coefficient of Water in Humidified Nitrogen, D_v

According to Blanc's law[39], the diffusion coefficient of water in a mixture of nitrogen and water (ie. humidifed nitrogen), D_v is estimated by

$$D_v = \left[\frac{x_v}{D_{vv}} + \frac{x_g}{D_{vg}}\right]^{-1} \quad (27)$$

Where D_{vv} is the self-diffusion coefficient of water vapour and D_{vg} is the diffusion coefficient of water vapour in nitrogen. As discussed in section 2.1.3, x_v equals 0.023 and 0 for 100% RH and 0% RH, respectively. The parametrizations of D_{vv} and D_{vg} are listed in Table 1. The D_{vg}/D_{vv} ratio at 293.15 K is calculated to be $2.49\times10^{-5}/1.64\times10^{-5}=1.52$ and hence the D_v/D_{vg} ratio across the whole humidity range (0 to 100%) varies between 0.988 and 1. Thus, even at 100% RH, the difference between D_v and D_{vg} is only 1.2%. Given that the dominant uncertainty in the value of D_v comes from the reported ±6% uncertainty in the value of D_{vg}[36], we approximate D_v with D_{vg} throughout this work without any significant loss of precision. The influence of the uncertainty in D_{vg} on the evaporation rate predicted

by the Kulmala, Liu and K-V-H models will be discussed later.

2.2.3 Thermal Conductivity of Humidified Nitrogen, *K*

The thermal conductivity (K) of a mixture, comprising two species with thermal conductivities K_v and K_g and partial pressure p_v and p_g respectively, is estimated from[40]

$$K = \frac{K_v}{1+0.556p_g/p_v} + \frac{K_g}{1+1.189p_v/p_g} \qquad (28)$$

In this study, K_v and K_g are the thermal conductivities of water vapour and nitrogen, respectively, which together make up a humidified nitrogen atmosphere. The expressions for K_v, determined by Sengers and Watson (1986)[41], and K_g, reported by Lemmon and Jacobsen (2004)[42], are listed in Table 1 and are recommended by Miles et al. (2012)[14]. Under the conditions investigated here (atmospheric pressure and 293.15 K), the calculated K_g/K ratio at a maximum RH of 100% is 0.998, meaning the value of K_g is only 0.2% less than the value of K, even for the highest partial pressure of water in the gas phase. As Lemmon and Jacobsen give the uncertainty in the value of K_g calculated using their parameterization as ± 2%, we have here used K_g instead of K in model predictions for convenience. From the expression of K_g in Table 1, coefficients K_0 and K_1 in Equation (14) are 3.9827×10^{-3} and 7.3167×10^{-5}, respectively. The influence of the ± 2% uncertainty in the value of K_g on the evaporation rate predicted by the different models will be discussed later.

2.3 Kinetic Parameters

2.3.1 The Mass Accommodation Coefficient, α_M, and Thermal Accommodation Coefficient, α_T

The Fuchs-Sutugin transitional correction factors for mass (β_M) and heat (β_T) transfer are defined by[16]

$$\beta_M = \frac{1+Kn_M}{1+\left(\frac{4}{3\alpha_M}+0.377\right)Kn_M+\frac{4}{3\alpha_M}Kn_M^2} \qquad (29)$$

$$\beta_T = \frac{1+Kn_T}{1+\left(\frac{4}{3\alpha_T}+0.377\right)Kn_T+\frac{4}{3\alpha_T}Kn_T^2} \qquad (30)$$

where $Kn_M = \lambda_M/r$ and $Kn_T = \lambda_T/r$ are the Knudsen numbers for mass and heat transfer, respectively. $\lambda_M = 3D_v/\overline{c}$ and $\lambda_T = 3K/\rho_g C_v \overline{c}$ are the mean free paths for mass and heat transfer, respectively. C_v is the specific heat capacity of gas at constant volume and is nearly constant within a narrow temperature range (743.2 J kg^{-1} K^{-1} at 293.15 K[37]). $\overline{c} = \sqrt{8RT/\pi M_g}$ is the average mean speed of gas molecules where M_g is the molar mass of the gas.

Previous studies have demonstrated that the α_M value of water should be greater than 0.5[14,20,43] and even close to unity[44,45]. The α_T value of water is usually assumed to be unity, which has been verified by numerical simulation and experimental results[17,46,47]. The effect of α_M on the model predictions is discussed later.

2.3.2 Thermal Diffusion Factor, α_D

When the evaporation process is slow, the temperature at the droplet surface remains close to the gas phase temperature. Thus, the mass flux component introduced by the temperature gradient (I_{c2} in Equation (7)) is very small, and the effect of α_D can be ignored. When the evaporation process is rapid and the suppression of the droplet surface temperature below the gas phase becomes large, I_2 becomes significant. The effect of the value of α_D on the mass flux during evaporation and condensation is illustrated in Figure 1. The evaporation/condensation process would be accelerated if $\alpha_D<0$ or decelerated if $\alpha_D>0$.

At present, the α_D value in the water vapour-nitrogen system is not well known. Different ranges of α_D

value have been estimated and reported, e.g., between -0.3 and 0.3[48], between -0.1 and 0.1[16], and between -0.034 and -0.024[34]. The effect of the value of α_D on the K-V-H model predictions will be discussed later and the plausible value of α_D will be presented.

3 Parameters Sensitivity Analysis and Model Comparison

3.1 Sensitivity Analysis of Parameters in the Kulmala, Liu and K-V-H Models

Previous studies have examined the sensitivity of the Kulmala model predictions to the value of α_M, and to the uncertainties in the values of D_v and K_g (± 6% and ± 2% respectively)[14]. These uncertainties have an impact on the estimation of the gas phase RH inferred from an evaporation rate measurement. The uncertainty using the Kulmala model is given by

$$RH_{Kulmala} = RH_{\mathrm{H2O}}{}^{+(0.169RH^2-0.364RH+0.194)}_{-(0.020RH+0.021)} \quad (31)$$

arising primarily from the uncertainty in D_v and K_g[29]. RH_{H2O} is the RH (expressed as a saturation) extracted assuming the values of K_g and D_v as calculated using the literature parameterisations. The uncertainty bounds on the RH value are then determined from considering D_v and K_g values where both are increased by their maximum uncertainty, or both decreased by their maximum uncertainty, impacting on the predicted evaporation rate.

In this work, we apply the same analysis approach to the Liu and K-V-H models, analyzing their sensitivity to the thermophysical and kinetic parameters identified in section 2.2 and 2.3. The sensitivity of the K-V-H model predictions to the value of α_M and α_D are discussed below; the sensitivity of the Liu model to the value of α_M has already been discussed in a previous publication[32]. The impact of the uncertainties in the parameters D_v and K_g (± 6% and ± 2%, respectively) were also determined for both

Liu and K-V-H models.

3.1.1 Thermal Diffusion Factor, α_D

Previous theoretical and experimental studies[20,21,24] have concluded that the Kulmala model is capable of accurately describing slow evaporation processes, i.e., the evaporation profile (radius vs time) of a water droplet evaporating at RH>80% when the suppression in droplet temperature is <3 K. Here, we use the Kulmala model to predict the radius of an evaporating water droplet as a function of time for a period of ~24 s, and then treat the prediction as a reference curve, as shown in Figures 2(a) and (b). The conditions used in the Kulmala simulation are: RH=90%, T_∞=293.15 K, V_g=0.03 m/s, r_0=25 μm, α_M=1 and α_T=1. The evaporation kinetics of a water droplet under the same conditions were predicted using the K-V-H model when varying α_D = 0, -0.2, -0.3, -0.4 and -0.5, as shown in Figure 2(a). It can be seen that the radius vs time curve predicted from the Kulmala model lies between the curves for α_D = -0.4 and -0.5 from the K-V-H model, with higher resolution simulations showing that α_D = -0.43 gives the best agreement between the two models. As expected, α_D = 0 shows a much slower droplet evaporation rate as it does not include the additional mass flux due to the temperature gradient between the droplet surface and the gas phase. As discussed in section 2.3.2, the evaporation process would be decelerated if α_D>0 and therefore these values are excluded from the comparison. A value for α_D of -0.43 is consistent with the negative values reported in previous studies[34].

3.1.2 Mass Accommodation Coefficient, α_M

By assuming α_D = -0.43, α_T = 1 and varying α_M = 0.1, 0.2, 0.5 and 1, we used the K-V-H model to predict the evaporation kinetics of a water droplet under the same conditions described in 3.1.1. As shown in

Figure 2(b), the predicted evaporation rate progressively decreases as α_M is reduced below 1, consistent with predictions from the reference Kulmala model. As with our earlier work, the difference between the K-V-H curves at α_M=0.5 and α_M=1 is too small to be resolved by the EDB measurement (where the accuracy in sizing is ± 100 nm). When the α_M value used in the K-V-H model decreases to 0.2 and 0.1, the droplet radius is overestimated significantly and this would be resolvable from the EDB measurements. As discussed in section 2.3.1, the α_M value should be greater than 0.5, hence, the effect of α_M in this range on the K-V-H model prediction can be ignored.

3.1.3 Uncertainties in D_v and K_g

The effect of uncertainties in the diffusion coefficient and thermal conductivity on predictions from the Liu and K-V-H models were investigated in two ways. First, their effect on the evaporation rate of a pure water droplet as predicted by the two models was determined by simulating evaporation profiles at a given RH using three sets of parameter combinations: (i) D_v and K_g values as given by the literature parameterisations; (ii) (1+0.06)×D_v and (1+0.02)×K_g; (iii) (1-0.06)×D_v and (1-0.02)×K_g. The results of the simulations are shown in Figure 3 for a range of RHs. The uncertainties in D_v and K_g have the largest impact on the Liu model, with the value of dr^2/dt changing by between ± 3 to 4% depending on the RH. The K-V-H model (using α_D = -0.43) is less susceptible to the uncertainties, with changes of between ± 1.5 and 2.75% depending on RH. The effect of the uncertainties on the evaporation rate predicted using the Kulmala model is also included for comparison. We restrict our calculations for this system to RH > 80%, recognizing the increasing errors in this model when pure water droplets evaporate at lower RHs leading to higher temperature suppressions.

In the second step in the analysis, the uncertainty in the RH that would be extracted from fitting a water droplet evaporation profile using the Liu and K-V-H models was determined when taking in to account the ±6% and ±2% uncertainties in D_v and K_g respectively. This is identical to the method used in the determination of equation (31) discussed previously for the Kulmala model. Water droplet evaporation profiles were measured at several relative humidities below 80% RH, with the Kulmala model used to simulate evaporation profiles at RHs above 80%. Each of these profiles was then fitted with three different versions of the Liu and K-V-H models: (i) with D_v and K_g as given in the parameterizations; (ii) with (1+0.06)×D_v and (1+0.02)×K_g; and (iii) with (1-0.06)×D_v and (1-0.02)×K_g. The results are shown in Figure 4. As would be expected given the results in Figure 3, the uncertainty in the retrieved RH is highest for the Liu model. The uncertainties in the RH extracted using the Liu and K-V-H models are given in equations (32) and (33) respectively, where the RH is given in the form of fractional saturation.

$$RH_{Liu} = RH_{\mathrm{H2O}}{}^{+\left(2.84E-4.RH^2-2.946E-2.RH+2.922E-2\right)}_{-\left(5.712E-4.RH^2-3.248E-2.RH+3.196E-2\right)} \quad (32)$$

$$RH_{KVH} = RH_{\mathrm{H2O}}{}^{+\left(6.0404E-3.RH^2-2.5803E-2.RH+1.9873E-2\right)}_{-\left(5.7067E-3.RH^2-2.7790E-2.RH+2.2087E-2\right)} \quad (33)$$

3.2 Comparison of the Evaporation Kinetics of a Water Droplet Predicted by the Kulmala, Liu and K-V-H Models

The evaporation kinetics of water droplets over an RH range of 0 - 90% were simulated using the Kulmala model, the Liu model and the K-V-H model in order to perform an intercomparison. Model parameters were fixed at T_∞=293.15 K, V_g=0.03 m/s, r_0=25 μm, α_M=1, α_T=1. The evaporation profiles at RH = 90%, 80%, 50%, 20% and 0% are shown in Figure 5. As expected, the droplet evaporation rate increases rapidly with decreasing RH. As before, the radius vs time curve at an RH=90% predicted by the Liu model, Figure 5(a), agrees well with the curve predicted by the Kulmala model (used as the

benchmark model), confirming the accuracy of the Liu model[32]. The prediction from the K-V-H model, assuming α_D = -0.43, similarly matches.

At RH=80%, the predicted radius from the Liu model is smaller than that from the Kulmala model but matches well with that from the K-V-H model, assuming α_D = -0.43, as shown in Figure 5(b). Indeed, under all conditions of RH<80%, the Kulmala model underestimates the evaporation rate and hence overestimates the droplet radius, diverging progressively further from the Liu and K-V-H models as the RH is reduced. This is due to the failure to properly treat the droplet surface temperature suppression during faster evaporation and indicates that the Kulmala model is not applicable in this RH range when considering measurements at 293.15 K. When the RH is reduced below 50 %, predictions from the Liu model are systematically at larger size at any time point when compared to K-V-H model although the models agree within their expected uncertainties, as shown in Figures 5(c), (d) and (e).

4 Using Water Probe Droplets to Determine RH over a Wide Range

To compare the ability of the Kulmala, Liu and K-V-H models to accurately predict the evaporation kinetics of a water droplet at a wide range of RHs and evaporation rates, a concentric cylinder electrodynamic balance (CK-EDB) was used to measure a series of water droplet evaporation profiles (radius vs time) for a range of RHs. These profiles were then used as test cases for performing model fits.

4.1 Experimental Description

The measurement procedure of the CK-EDB single particle technique is described in detail

elsewhere[18,21,29] and is described only briefly here. The CK-EDB instrument, comprising two pairs of cylindrical electrodes in a concentric arrangement, is operated under atmospheric pressure. A dry nitrogen flow, with flow rate Q_{dry} controlled by a Mass Flow Controller (MFS; MKS 1179A), and a humidified nitrogen flow, with flow rate Q_{wet} controlled by a second MFS, are mixed together and continuously introduced into the EDB chamber from below through the annulus formed between the inner and outer electrode. This allows evaporating droplets to be exposed to gas phase humidities from >97% RH down to dry conditions. The temperature of the trapping chamber is precisely controlled by a recirculating chiller (Julabo, F32) and can be measured in situ with a temperature probe. The coolant bath was set at 293.15 K for all reported measurements in this work. Single droplets generated on-demand by a microdispenser (Microfab MJ-ABP-01) are charged by an induction electrode and injected into the chamber, becoming trapped within the electrical field at the central null-position of the trapping electrodes. The droplet is illuminated by a laser beam with wavelength 532 nm and the resulting elastically scattered light is collected as a function of angle to generate a phase function which consists of a series of light and dark fringes generated by constructive and destructive interference. The fringe spacing is used along with the Geometrical Optics Approximation to calculate the droplet radius every 10 ms with an accuracy of ± 100 nm[18,49]. During the measurement, a levitated droplet remains spherical as it remains sufficiently small that the capillary force dominates the gravitational force[50].

4.2 Measurement of the Evaporation Profiles of Water Droplets under Different Gas Flow Mixing Ratios and Determination of the Corresponding RH

By keeping the total gas flow, $Q_{total}(=Q_{wet}+Q_{dry})$, at 200 cm^3/min and varying the Q_{wet} /Q_{total} ratio at 0.8, 0.7, 0.6, 0.5, 0.4, 0.3 and 0.2, the evaporation profiles of water droplets evaporating under a range of

different RH conditions were measured. Ten water droplet evaporation profiles were recorded at each RH to examine the reproducibility of the measurements and are shown in Figure 6(a).

The intercomparison of the three models proceeded as follows. The Kulmala, Liu and K-V-H models were used to simulate evaporation profiles over a wide range of RHs. These were then compared to the experimental evaporation curves in order to obtain the best fit value of RH as a function of Q_{wet}/Q_{total} ratio, recognizing that high quality fits could be achieved in each case (example fit shown in Figure 6(b)). The inferred RHs are shown in Figure 6(c). When the Q_{wet}/Q_{total} ratio is below 0.7, the RH predicted by the Kulmala model begins to deviate from the linear relationship expected between the RH and Q_{wet}/Q_{total} ratio, with the deviation increasing with decreasing Q_{wet}/Q_{total} ratio. This is due to the inherent problems in the Kulmala model when the droplet surface temperature suppression increases beyond 3 K. Once again this shows that this model is not suitable for accurate determination of low RH values. The RH values predicted by the Liu model and the K-V-H model agree well with each other, and follow the expected linear relationship between RH and Q_{wet}/Q_{total} ratio. The three models do not agree with the 1:1 line shown on the figure as even on full wet flow (i.e. $Q_{wet}/Q_{total} = 1$) it would not be possible to generate an RH of 100%. At 20% RH, the surface temperature suppression predicted by the Liu and K-V-H models is 12.10 and 11.95 K respectively.

4.3 Comparison of RH Determined by NaCl and $NaNO_3$ Probe Equilibrium Size Method and Water Probe Method Proposed in this Work

We now further verify the accuracy of the Liu and K-V-H models for the simulation of the evaporation kinetics of pure water droplets under high mass flux conditions (low RH) where the temperature

suppression is large. Implicitly, this is also equivalent to verifying the accuracy of these models for determining the gas phase RH using water probe droplets at low humidities[21]. To achieve this, we utilized the CK-EDB to alternately measure the evaporation kinetics of aqueous NaCl or aqueous $NaNO_3$ droplets and water droplets. The equilibrated radius of the aqueous NaCl probe droplets (with initial concentration of 125.01 g/L, a water activity of 0.923) was used to determine the gas phase RH at humidities greater than 50%, while equilibration of aqueous $NaNO_3$ probe droplets (with initial concentration of 86.13 g/L, a water activity of 0.914) was used to determine humidities below 50%. $NaNO_3$ was used in addition to NaCl as the latter effloresces at ~45% RH[51] and thus could not be used for the low humidity measurements.

Multiple droplet evaporation profiles were recorded at a series of relative humidities between 10% and 80% RH, with the total gas flow, Q_{total}, kept constant in each measurement at 200 cm^3 /min (an example of a typical measurement is shown in Figure 7). The Liu model and the K-V-H model were then used to fit the experimental water droplet evaporation profiles (assuming $\alpha_M = 1$, $\alpha_T = 1$ and $\alpha_D = -0.43$) to extract the value of the relative humidity. These values were compared with the reference RH as well as the RH retrieved when using the Kulmala model, in order to show the level of improvement achievable with the proposed models.

The values of the RH fitted by the two models as well as the reference RH values determined by the NaCl or $NaNO_3$ droplet equilibrium size method are illustrated in Table 2 and Figure 8 for comparison. The uncertainty in the RH retrieved using the NaCl probe droplet (arising from uncertainties in the initial droplet size, composition and equilibrated radius) has previously been reported and is given in

equation (34). Here we assume the uncertainty in the RH retrieved by the $NaNO_3$ droplets to be of a similar magnitude.[29]

$$RH_{eq} = RH_{\mathrm{NaCl}}{}^{+\left(-0.0175RH^2-0.0005RH+0.017\right)}_{-\left(-0.0266RH^2+0.0086RH+0.017\right)} \quad (34)$$

To test the accuracy of the Liu and K-V-H models at RHs > 80%, Kulmala model simulations were performed for 85% RH and 95% RH and these were used as benchmark evaporation profiles to be fitted by the Liu and K-V-H models. The results are also shown in Table 2 and Figure 8.

The data shows that the Liu and K-V-H models are both able to accurately represent the evaporation kinetics of water droplets over a wide mass flux range. From 95% RH down to ~40 % RH, both model predictions show excellent agreement with the reference RH within its stated uncertainties. In contrast, fits performed using the Kulmala model start to deviate from the reference values below 60% RH. As the Kulmala model underestimates the droplet mass flux for a given humidity, a lower RH value is required to fit the experimental time-dependent radius curve. Below 40% RH, the Liu and K-V-H models begin to slightly underpredict the RH (indicating that they too also underpredict the droplet mass flux in this RH range); however, the level of agreement is still good, with a maximum deviation in RH of less than 7% for the Liu model and less than 5% for the K-V-H model at the lowest humidity tested. While both models agree well with the reference values over the whole RH range, the K-V-H model has a slightly better accuracy and higher precision than the Liu model, although the latter does have the advantage that it does not require the value of an additional correction parameter (the thermal diffusion factor α_D) to be accurately known. Therefore, comparing with the equilibrium size method using aqueous salt droplet[52] (i.e., NaBr[53], NaCl[29]) and acid droplet (i.e., H_2SO_4[54]), the water probe method based on the proposed models is convenient for accurate determination of RH in wide range

which is essential for hygroscopiticy measurement.

5 Conclusions

Quantifying the rates of evaporation and condensation of water (and indeed other condensable volatile components) from aerosol particles is important in a broad range of applications from predicting droplet drying rates through to the kinetics of activation of cloud condensation nuclei and the formation of cloud droplets. Dependent on the relative rates of mass and heat flux, changes in droplet temperature can be substantial in early stages of the evaporation or condensation process, leading to an aerosol particle with a temperature suppressed below that of the ambient gas in evaporative cooling or above the ambient gas due to the latent heat generated on condensation. We have compared the performance of three treatments of the condensation/evaporation microphysics, comparing model predictions for the evaporation of pure water droplets. We have also considered in detail the sensitivity of model predictions to uncertainties in the thermophysical properties required to simulate water droplet evaporation and condensation.

Specifically, we have used the Kulmala model, the Liu model and the K-V-H model to predict the evaporation kinetic of water droplet under given conditions and RH from 0% and 90% for model comparison. The time-dependent radii predicted from all three models are in good agreement for RH>90%. However, at lower RH, and thus for high rates of evaporation and large degrees of evaporative cooling (i.e. between 20% and 90% RH), predictions from the Liu and the K-V-H models continue to agree but diverge from the Kulmala model, which provides an underestimate of the evaporative flux, failing to account fully for the degree of evaporative cooling.

Finally, we utilized the EDB technique to measure the evaporation kinetics of water droplet under different RHs (as implemented from a variation in humidified and dry nitrogen gas flow rates, Q_{wet}/Q_{total}), estimating the corresponding RH from the evaporation rate of a pure water droplet using the Liu model and the K-V-H model. A linear relationship between the predicted RH and the setting value of Q_{wet}/Q_{total} ratio is observed over a wide RH range down to ~20%. Furthermore, we used the Comparative-Kinetics EDB technique to measure the evaporation profiles of aqueous NaCl and aqueous $NaNO_3$ droplets, and water droplets alternately, and compared the RH values predicted by the proposed water probe method with the reference values estimated from the NaCl or $NaNO_3$ probe equilibrium size method (RH range 10% - 95%). The results from the two methods show excellent agreement within the uncertainty of the measurements at RHs > 40%, with a small underprediction of the mass flux seen at RHs < 40% (equivalent to less than 7% difference in RH retrieved by the Liu model and less than 5% difference in RH for the K-V-H model at the lowest humidity). We conclude that the Liu and K-V-H models are able to accurately represent the evaporation kinetics (and, thus, also condensation) of aerosol droplets of volatility similar to pure water over broad ranges of environmental conditions and evaporation rates. In future, we will explore the accuracy of these treatments for other volatile solvents and for the evaporation of water droplets at much higher temperatures.

Acknowledgements

This work is financially supported by the National Key Foundation for Exploring Scientific Instrument of China (No.2013YQ47078105). JPR and REHM acknowledge financial support from the EPSRC through grant EP/N025245/1. Florence Gregson and Tom Hilditch are acknowledged for their collection

of the $NaNO_3$ probe droplet data.

References

1 A. S. Mujumdar, *Handbook of Industrial Drying*, CRC Press, Taylor & Francis Group, Boca Raton, FL, 1988, vol. 6.

2 U. Pöschl, Atmospheric aerosols: Composition, transformation, climate and health effects, *Angew. Chemie - Int. Ed.*, 2005, **44**, 7520–7540.

3 H. Vehkamäki and I. Riipinen, Thermodynamics and kinetics of atmospheric aerosol particle formation and growth, *Chem. Soc. Rev.*, 2012, **41**, 5160.

4 J. Tröstl, W. K. Chuang, H. Gordon, M. Heinritzi, C. Yan, U. Molteni, L. Ahlm, C. Frege, F. Bianchi, R. Wagner, M. Simon, K. Lehtipalo, C. Williamson, J. S. Craven, J. Duplissy, A. Adamov, J. Almeida, A. K. Bernhammer, M. Breitenlechner, S. Brilke, A. Dias, S. Ehrhart, R. C. Flagan, A. Franchin, C. Fuchs, R. Guida, M. Gysel, A. Hansel, C. R. Hoyle, T. Jokinen, H. Junninen, J. Kangasluoma, H. Keskinen, J. Kim, M. Krapf, A. Kürten, A. Laaksonen, M. Lawler, M. Leiminger, S. Mathot, O. Möhler, T. Nieminen, A. Onnela, T. Petäjä, F. M. Piel, P. Miettinen, M. P. Rissanen, L. Rondo, N. Sarnela, S. Schobesberger, K. Sengupta, M. Sipilä, J. N. Smith, G. Steiner, A. Tomè, A. Virtanen, A. C. Wagner, E. Weingartner, D. Wimmer, P. M. Winkler, P. Ye, K. S. Carslaw, J. Curtius, J. Dommen, J. Kirkby, M. Kulmala, I. Riipinen, D. R. Worsnop, N. M. Donahue and U. Baltensperger, The role of low-volatility organic compounds in initial particle growth in the atmosphere, *Nature*, 2016, **533**, 527–531.

5 H. D. C. Smyth and A. J. Hickey, *Controlled Pulmonary Drug Delivery*, Springer, London, 2011.

6 Á. Farkas, D. Lewis, T. Church, A. Tweedie, F. Mason, A. E. Haddrell, J. P. Reid, A. Horváth and I. Balásházy, Experimental and computational study of the effect of breath-actuated mechanism built in the NEXThaler® dry powder inhaler, *Int. J. Pharm.*, 2017, **533**, 225–235.

7 A. E. Haddrell, D. Lewis, T. Church, R. Vehring, D. Murnane and J. P. Reid, Pulmonary aerosol delivery and the importance of growth dynamics, *Ther. Deliv.*, 2017, **8**, 1051–1061.

8 A. H. Persad and C. A. Ward, Expressions for the Evaporation and Condensation Coefficients in the Hertz-Knudsen Relation, *Chem. Rev.*, 2016, **116**, 7727–7767.

9 R. Marek and J. Straub, Analysis of the evaporation coefficient and the condensation coefficient of water, *Int. J. Heat Mass Transf.*, 2001, **44**, 39–53.

10 B. Y. H. Liu, D. Y. H. Pui, K. T. Whitby, D. B. Kittelson, Y. Kousaka and R. L. McKenzie, The aerosol mobility chromatograph: A new detector for sulfuric acid aerosols, *Atmos. Environ.*, 1978, **12**, 99–104.

11 M. N. Chan, M. Y. Choi, N. L. Ng and C. K. Chan, Hygroscopicity of water-soluble organic compounds in atmospheric aerosols: Amino acids and biomass burning derived organic species, *Environ. Sci. Technol.*, 2005, **39**, 1555–1562.

12 E. J. Davis and A. K. Ray, Single aerosol particle size and mass measurements using an electrodynamic balance, *J. Colloid Interface Sci.*, 1980, **75**, 566–576.

13 R. E. H. Miles, K. J. Knox, J. P. Reid, A. M. C. Laurain and L. Mitchem, Measurements of mass and heat transfer at a liquid water surface during condensation or evaporation of a

subnanometer thickness layer of water, *Phys. Rev. Lett.*, 2010, **105**, 1–4.
14 R. E. H. Miles, J. P. Reid and I. Riipinen, Comparison of approaches for measuring the mass accommodation coefficient for the condensation of water and sensitivities to uncertainties in thermophysical properties, *J. Phys. Chem. A*, 2012, **116**, 10810–10825.
15 N. A. Fuchs, *Evaporation and Droplet Growth in Gaseous Media*, Pergamon Press, London, Oxford, New York, Paris, 1959.
16 P. E. Wagner, *Aerosol Microphysics. II: Chemical Physics of Microparticles*, Springer-Verlag, Berlin, Heidelberg, New York, 1982.
17 R. Hołyst, M. Litniewski, D. Jakubczyk, M. Zientara and M. Woźniak, Nanoscale transport of energy and mass flux during evaporation of liquid droplets into inert gas: computer simulations and experiments, *Soft Matter*, 2013, **9**, 7766.
18 J. F. Davies, A. E. Haddrell and J. P. Reid, Time-resolved measurements of the evaporation of volatile components from single aerosol droplets, *Aerosol Sci. Technol.*, 2012, **46**, 666–677.
19 J. F. Davies, R. E. H. Miles, A. E. Haddrell and J. P. Reid, Influence of organic films on the evaporation and condensation of water in aerosol, *Proc. Natl. Acad. Sci.*, 2013, **110**, 8807–8812.
20 J. F. Davies, R. E. H. Miles1, A. E. Haddrell and J. P. Reid, Temperature dependence of the vapor pressure and evaporation coefficient of supercooled water, *J. Geophys. Res. Atmos.*, 2014, **119**, 10931–10940.
21 G. Rovelli, R. E. H. Miles, J. P. Reid and S. L. Clegg, Accurate Measurements of Aerosol Hygroscopic Growth over a Wide Range in Relative Humidity, *J. Phys. Chem. A*, 2016, **120**, 4376–4388.
22 G. Rovelli, E. H. R. Miles, P. J. Reid and L. S. Clegg, Hygroscopic properties of aminium sulfate aerosols, *Atmos. Chem. Phys.*, 2017, **17**, 4369–4385.
23 A. Marsh, R. E. H. Miles, G. Rovelli, A. G. Cowling, L. Nandy, C. S. Dutcher and J. P. Reid, Influence of organic compound functionality on aerosol hygroscopicity: Dicarboxylic acids, alkyl-substituents, sugars and amino acids, *Atmos. Chem. Phys.*, 2017, **17**, 5583–5599.
24 M. Kulmala, T. Vesala and P. E. Wagner, An Analytical Expression For the Rate of Binary Condensational Particle Growth, *Proc. R. Soc. A Math. Phys. Eng. Sci.*, 1993, **441**, 589–605.
25 J. H. Seinfeld and S. N. Pandis, *Atmospheric Chemistry and Physics- From Air Pollution to Climate Change*, John Wiley & Sons, Inc., Hoboken, New Jersey, Second., 2006.
26 K. M. Jakubczyk, Daniel, Derkachov G, Do Duc Tho, Kolwas Krystyna, Coefficients of evapoartion and gas phase diffusion of low-volatility organic solvents in nitfogen from study of evaporating droplets, *J. Phys. Chem. A*, 2010, **114**, 3483–3488.
27 E. J. Davis, A history of single aerosol particle levitation, *Aerosol Sci. Technol.*, 1997, **26**, 212–254.
28 E. J. Davis, Electrodynamic Levitation of Particles, *Aerosol Meas. Princ. Tech. Appl. Third Ed.*, 2011, 417–434.
29 J. F. Davies, A. E. Haddrell, A. M. J. Rickards and J. P. Reid, Simultaneous analysis of the equilibrium hygroscopicity and water transport kinetics of liquid aerosol, *Anal. Chem.*, 2013, **85**, 5819–5826.
30 M. Kulmala, T. Vesala and P. E. Wagner, An analytical expression for the rate of binary condensational particle growth: Comparison with numerical results, *J. Aerosol Sci.*, 1992, **23**, 133–136.

31 K. H. Ahn and B. Y. H. Liu, Particle activation and droplet growth processes in condensation nucleus counter-I. Theoretical background, *J. Aerosol Sci.*, 1990, **21**, 249–261.
32 Y. Y. Su, A. Marsh, A. E. Haddrell, Z. M. Li and J. P. Reid, Evaporation Kinetics of Polyol Droplets: Determination of Evaporation Coefficients and Diffusion Constants, *J. Geophys. Res. Atmos.*, 2017, **122**, 12,317-12,334.
33 M. Kulmala and T. Vesala, Condensation in the Continuum Regime, *J. Aerosol Sci.*, 1991, **22**, 337–346.
34 S. Heidenreich, Condensational droplet growth in the continuum regime--a critical review for the system air-water, *J. Aerosol Sci.*, 1994, **25**, 49–59.
35 T. R. Marrero and E. A. Mason, Gaseous Diffusion Coefficients, *J. Phys. Chem. Ref. Data*, 1972, **1**, 3–118.
36 W. J. Massman, A review of the molecular diffusivities of H2O, CO2, CH4, CO, O3, SO2, NH3, N2O, NO, and NO2in air, O2and N2near STP, *Atmos. Environ.*, 1998, **32**, 1111–1127.
37 W. M. Haynes, CRC Handbook of Chemistry and Physics, *Handb. Chem. Phys.*, , DOI:10.1136/oem.53.7.504.
38 D. M. Murphy and T. Koop, Review of the vapour pressures of ice and supercooled water for atmospheric applications, *Q. J. R. Meteorol. Soc.*, 2005, **131**, 1539–1565.
39 B. E. Poling, J. M. Prausnitz and J. P. O'Connell, *The properties of gases and liquids*, McGraw-Hill Book Company, New York, Fifth Edit., 2001.
40 A. L. Lindsay and L. A. Broiiley, Thermal Conductivity of Gas Mixtures, *Ind. Eng. Chem.*, 1950, **42**, 1508–1511.
41 J. V. Sengers and J. T. R. Watson, *J. Phys. Chem. Ref. Data*, 1986, 15, 1291–1314.
42 E. W. Lemmon and R. T. Jacobsen, Viscosity and thermal conductivity equations for nitrogen, oxygen, argon, and air, *Int. J. Thermophys.*, 2004, **25**, 21–69.
43 J. D. Smith, C. D. Cappa, W. S. Drisdell, R. C. Cohen and R. J. Saykally, Raman thermometry measurements of free evaporation from liquid water droplets, *J. Am. Chem. Soc.*, 2006, **128**, 12892–12898.
44 P. M. Winkler, A. Vrtala, R. Rudolf, P. E. Wagner, I. Riipinen, T. Vesala, K. E. J. Lehtinen, Y. Viisanen and M. Kulmala, Condensation of water vapor: Experimental determination of mass and thermal accommodation coefficients, *J. Geophys. Res. Atmos.*, 2006, **111**, 1–12.
45 J. Julin, M. Shiraiwa, R. E. H. Miles, J. P. Reid, U. Pöschl and I. Riipinen, Mass accommodation of water: Bridging the gap between molecular dynamics simulations and kinetic condensation models, *J. Phys. Chem. A*, 2013, **117**, 410–420.
46 P. M. Winkler, A. Vrtala, P. E. Wagner, M. Kulmala, K. E. J. Lehtinen and T. Vesala, Mass and thermal accommodation during gas-liquid condensation of water, *Phys. Rev. Lett.*, 2004, **93**, 1–4.
47 M. Zientara, M., Jakubczyk, D., Kolwas, K., Kolwas, Temperature dependence of the evaporation coefficient of water in air and nitrogen under atmospheric pressure: Study in water droplets, *J. Phys. Chem. A*, 2008, **112**, 5152–5158.
48 D. A. Frank-Kamenetskii, *Diffusion and heat transfer in chemical kinetics*, Plenum Press, New York, 2nd enl. a., 1969.
49 W. J. Glantschnig and S. H. Chen, Light scattering from water droplets in the geometrical optics approximation., *Appl. Opt.*, 1981, **20**, 2499–2509.
50 J. P. Reid, B. J. Dennis-Smither, N.-O. A. Kwamena, R. E. H. Miles, K. L. Hanford and C. J.

Homer, The morphology of aerosol particles consisting of hydrophobic and hydrophilic phases: hydrocarbons, alcohols and fatty acids as the hydrophobic component, *Phys. Chem. Chem. Phys.*, 2011, **13**, 15559.

51 Y. Gao, S. B. Chen and L. E. Yu, Efflorescence relative humidity of airborne sodium chloride particles: A theoretical investigation, *Atmos. Environ.*, 2007, **41**, 2019–2023.

52 M. D. Cohen, R. C. Flagan and J. H. Seinfeld, Studies of Concentrated Electrolyte Solutkns Using the Electrodynamic Balance. 1. Water Activities for Single-Electrolyte Solutions, *J. Phys. Chem.*, 1987, **91**, 4563–4574.

53 M. Y. Choi and C. K. Chan, Continuous Measurements of the Water Activities of Aqueous Droplets of Water-Soluble Organic Compounds, *J. Phys. Chem. A*, 2002, **106**, 4566–4572.

54 Z. Liang and C. K. Chan, A fast technique for measuring water activity of atmospheric aerosols, *Aerosol Sci. Technol.*, 1997, **26**, 255–268.

55 W. Wagner and A.Pruss, International Equations for the Saturation Properties of Ordinary Water Substance. Revised According to the International Temperature Scale of 1990. Addendum to J. Phys. Chem. Ref. Data 16, 893 (1987), *J. Phys. Chem. Ref. Data*, 1993, **22**, 783–787.

TABLES

Table 1. The thermophysical properties of water and nitrogen used in this work.

Parameter	Expression	Ref.
$\ln(p_{eq})$ / Pa	$54.842763-6763.22/T-4.210\cdot\ln(T)+0.000367\cdot T+\tanh\{0.0415(T-218.8)\}(53.878-1331.22/T-9.44523\cdot\ln(T)+0.014025\cdot T)$	38
$D_{v,g}$ / m^2 s^{-1}	$2.190\times10^{-5}\cdot\left(\frac{T}{273.15}\right)^{1.81}$	36
$D_{v,v}$ / m^2 s^{-1}	$7.5695\times10^{-10}\cdot T^{1.7575}$	14
ρ / kg m^{-3}	$(-1.23824054\times10^{-11}.T^6)+(2.22619377\times10^{-8}.T^5)+(-1.68379401\times10^{-5}.T^4)+(6.88300205\times10^{-3}.T^3)+(-1.61288564.T^2)+(0.206466342\times10^{2}.\mathrm{T})+(-1.03070991\times10^{4})$	55
L / J kg^{-1}	$3.14566\times10^{6}-2361.64\cdot T$	44
K_v / W K^{-1} m^{-1}	$0.01695-5.1478\times10^{-5}.T+1.89622\times10^{-7}.T^2$	41
K_g / W K^{-1} m^{-1}	$3.9827\times10^{-3}+7.3167\times10^{-5}.T$	42

Table 2. Tabulated data from Figure 8. First two columns give the RH and error range from the reference technique (Kulmala for RH >80%, equation 30; NaCl probe method for 50%< RH <80% and $NaNO_3$ probe method for RH < 50%, equation 33). Estimations of RHs and associated RH error ranges from the Liu and K-V-H models are then shown. The final two columns give the difference between the RH extracted using the Liu and K-V-H models and the reference RH.

Reference RH values		Liu model fits to water droplet evaporation		K-V-H model fits to water droplet evaporation		Deviation of model fits from reference RH / %	
RH_{ref} / %	RH_{ref} error range / %	RH_{Liu} / %	RH_{Liu} error range / %	RH_{KVH} / %	RH_{KVH} error range / %	Liu	K-V-H
95	94.80 – 95.07	94.95	94.79 – 95.10	94.96	94.88 – 95.04	-0.05	-0.04
85	84.60 – 85.67	85.14	84.66 – 85.58	85.19	84.94 – 85.42	+0.14	+0.19
70.08	69.08 – 70.89	71.1	70.15 – 71.97	71.36	70.84 -71.81	+1.02	+1.28
63.33	62.15 – 64.30	64.16	62.98 – 65.25	64.46	63.81 -65.04	+0.83	+1.13
56.20	54.86 – 57.32	56.82	55.46 – 58.07	57.2	56.39 – 57.91	+0.62	+1.00
42.50	40.92 - 43.86	42.90	41.09 – 44.56	43.76	42.66 – 44.73	+0.40	+1.26
32.50	30.80 – 34.00	28.99	26.73 – 31.06	30.39	28.97 – 31.65	-3.51	-2.11
22.90	21.14 – 24.50	16.04	13.36 – 18.49	18.10	16.38 – 19.64	-6.86	-4.80
11.00	8.80 – 12.67*	4.03	0.97 – 6.83	6.83	4.81 – 8.19	-6.97	-4.17

* RH_{ref} error range given by variability in repeat measurements, which was larger than the uncertainty range calculated using equation 34.

FIGURES

Figure 1. Analysis of the effect of the α_D range on the mass flux in both evaporation and condensation processes.

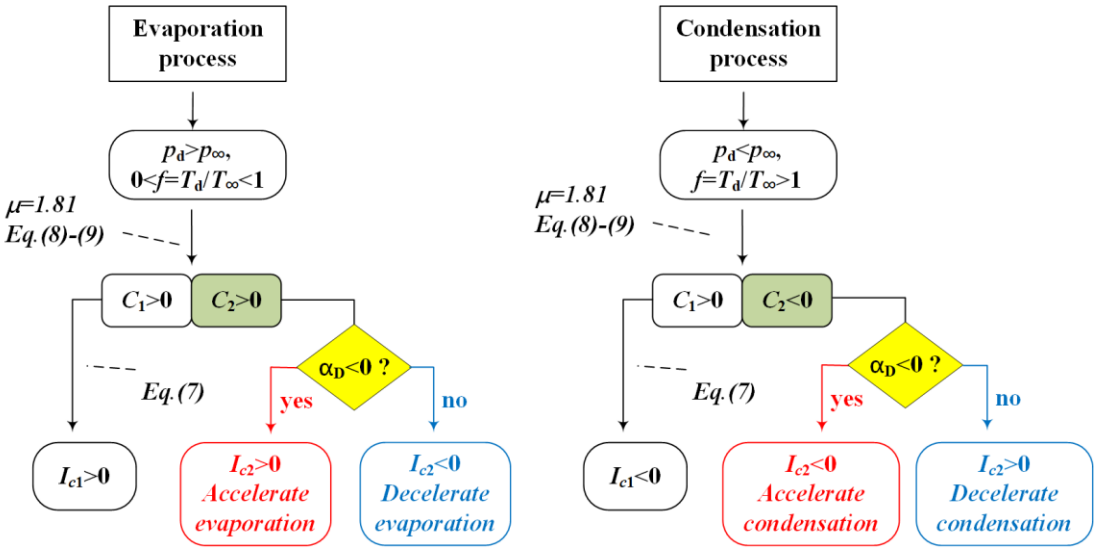

$I_{c1}>0$ or $I_{c2}>0$: the mass is transferred off the droplet.

Figure 2. (a) Comparison of the evaporation profiles of pure water droplets at 90% RH and 293.15 K predicted by the Kulmala model (black) and the K-V-H model when α_D is set as 0 (red), -0.2 (blue), -0.3 (green), -0.4 (orange) and -0.5 (purple). In all cases $\alpha_M = 1$, $\alpha_T = 1$ and V_g =0.03 m/s. Grey shading denotes a radius error of ± 100 nm, typical for the EDB. (b) Comparison of the evaporation profiles of pure water droplets at 90% RH and 293.15 K predicted by the Kulmala model (black) and the K-V-H model when α_M is set as 0.1 (red), 0.2 (blue), 0.5 (green) and 1 (orange). In all cases $\alpha_D = -0.43$, $\alpha_T = 1$ and V_g=0.03 m/s.

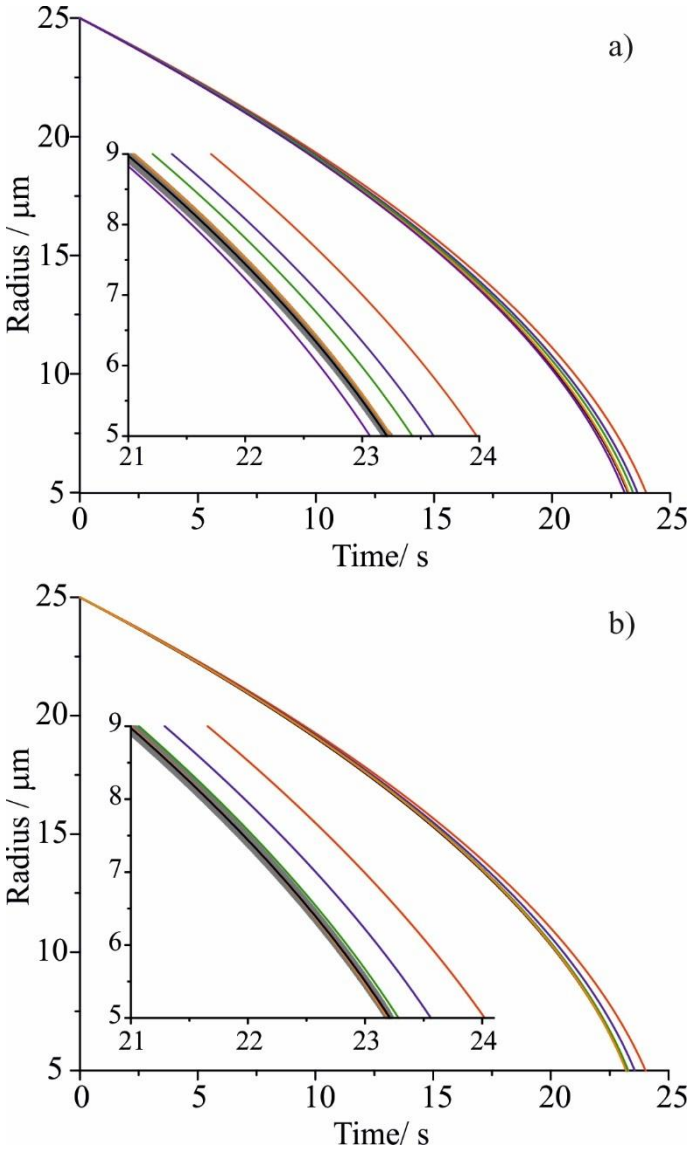

Figure 3. The percentage difference in the evaporation rate of pure water droplets (represented by the change in radius squared with time) when the uncertainties in the parameters D_{vg} and K_g are considered when simulating droplet evaporation for the K-V-H model (circles, red), Liu model (squares, black) and Kulmala model (triangles, blue). Filled symbols: +6% D_{vg} and +2% K_g; empty symbols: -6% D_{vg} and -2% K_g.

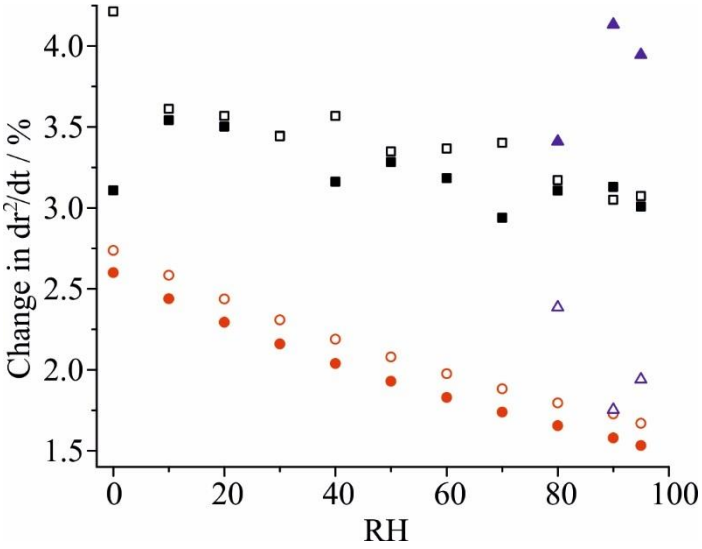

Figure 4. The absolute uncertainty in the RH retrieved by each model from an evaporation profile (radius vs time) for an evaporating water droplet in the RH range 20% to 95%. The uncertainty arises from the uncertainties in the values of the diffusion coefficients and thermal conductivities. Models: Liu, black; K-V-H (α_D = -0.43), red; Kulmala, blue.

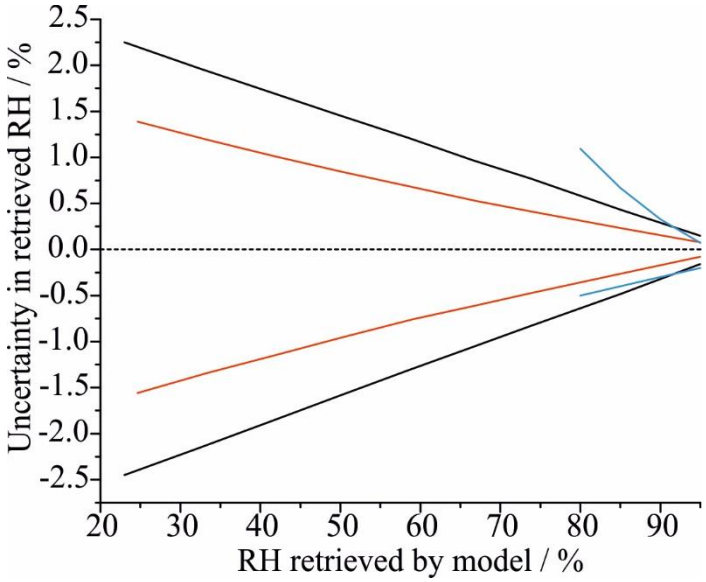

Figure 5. The predicted evaporation profiles of water droplet at RHs of (a) 90%, (b) 80%, (c) 50%, (d) 20% and (e) 0%; Liu model (black), K-V-H model (red) and Kulmala model (blue). Shaded region shows the error related to the uncertainty in the values of D_v and K_g.

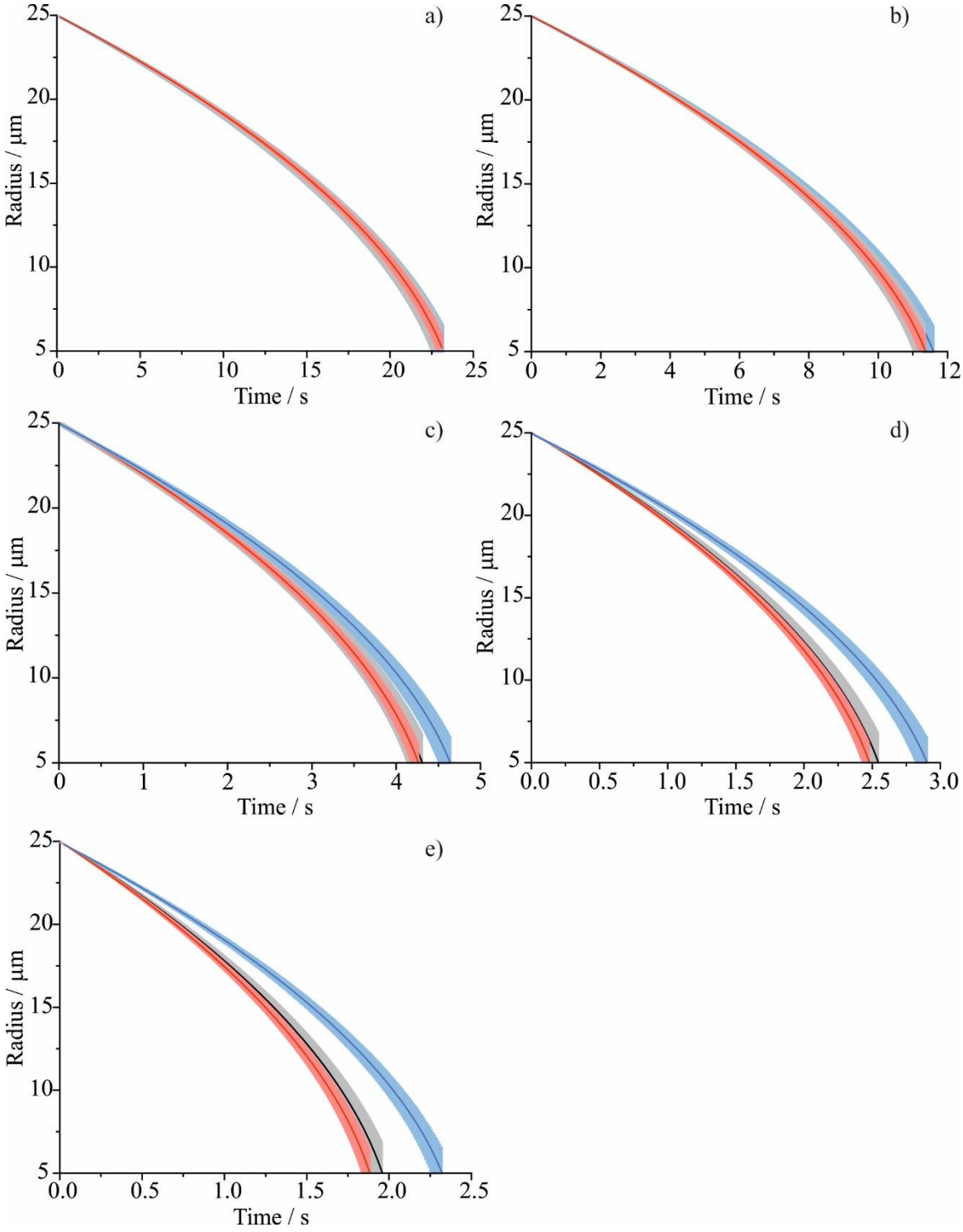

Figure 6. (a) The measured evaporation profiles of water droplets under different Q_{wet}/Q_{total} ratio conditions (left to right, Q_{wet}/Q_{total} ratio: 0.2, black; 0.3, red; 0.4, blue; 0.5, green; 0.6, orange; 0.7, pink; 0.8, purple). (b) Comparison of Liu model fit (22.66% RH) with experimental data for Q_{wet}/Q_{total} = 0.2. c) The RH (expressed as saturation) retrieved by the three models for each Q_{wet}/Q_{total} ratio (Kulmala, blue; Liu, black; K-V-H (α_d = -0.43), red). The error bars show the uncertainty in the retrieved RH. The solid grey line shows a linear fit through the Liu and K-V-H data. A dashed grey 1:1 line is shown for comparison.

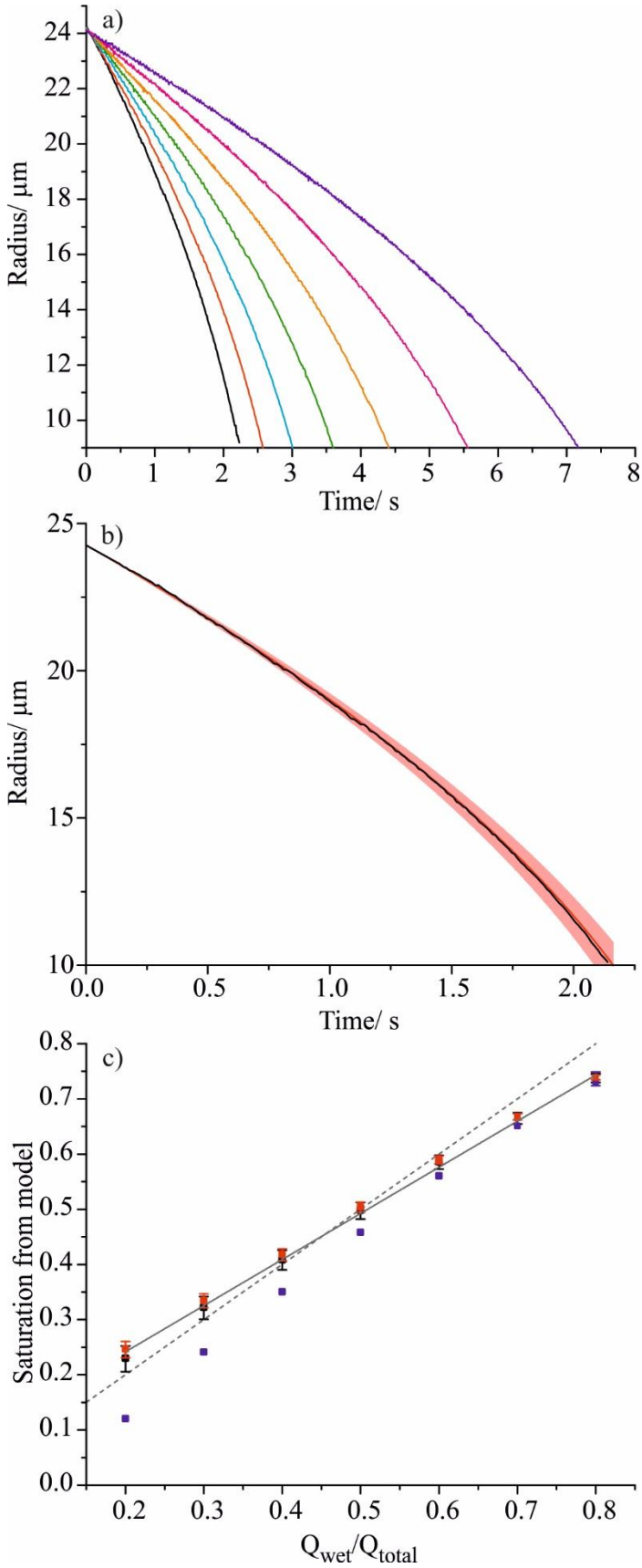
a)
Radius/ µm
Time/ s
b)
Radius/ µm
Time/ s
c)
Saturation from model
Q_{wet}/Q_{total}

Figure 7. Radius vs time profiles for a series of aqueous NaCl (red) and water droplets (black) evaporating in the CK-EDB at 293.15 K and Q_{wet}/Q_{total} = 0.8.

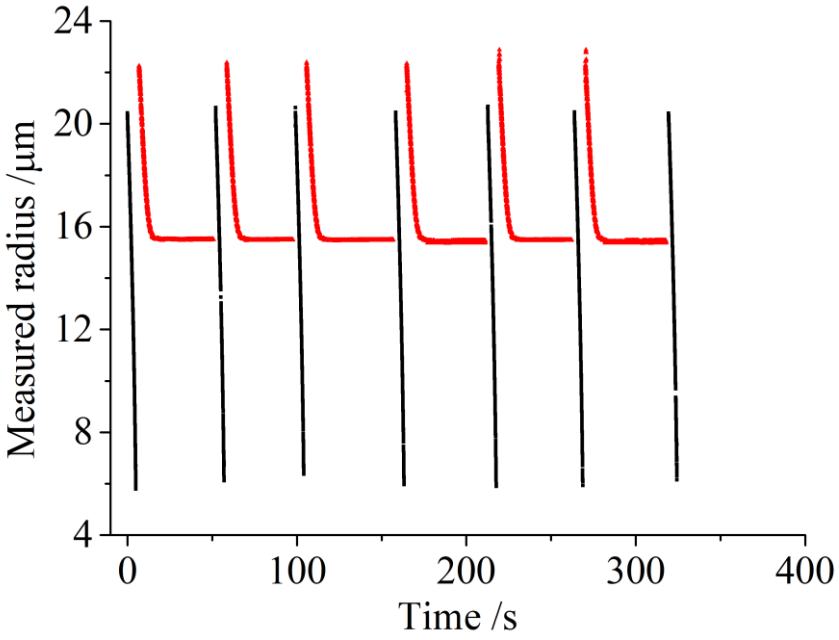

Figure 8. Comparison between the reference RH from the Kulmala model (RH>80%), sodium chloride probe droplets (50% < RH < 80%), and sodium nitrate probe droplets (RH < 50%), and the RH retrieved by the Liu (black), K-V-H (red) and Kulmala (blue) models. 1:1 line is shown for comparison.